

Accepted for publication by the Astrophysical Journal

Mid-Infrared Imaging of NGC 6334 I

James M. De Buizer^{1,2}, James T. Radomski³, Robert K. Piña^{2,3}, and Charles M. Telesco³

ABSTRACT

We present high-resolution ($<0''.5$) mid-infrared Keck II images of individual sources in the central region of NGC 6334 I. We compare these images to images at a variety of other wavelengths from the near infrared to cm radio continuum and speculate on the nature of the NGC 6334 I sources. We assert that the cometary shape of the UCHII region here, NGC 6334 F, is due to a champagne-like flow from a source on the edge of a molecular clump and not a due to a bow shock caused by the supersonic motion of the UCHII region through the interstellar medium. The mid-infrared emission is concentrated into an arc of dust that define the boundary between the UCHII region and the molecular clump. This dust arc contains a majority of the masers in the region. We discuss the nature of the four near-infrared sources associated with IRS-I 1, and suggest that one of the sources, IRS1E, is responsible for the heating and ionizing of the UCHII region and the mid-infrared dust arc. Infrared source IRS-I 2, which has been thought to be a circumstellar disk associated with a linear distribution of methanol masers, is found not to be directly coincident with the masers and elongated at a much different position angle. IRS-I 3 is found to be an extended source of mid-infrared emission coming from a cluster of young dusty sources seen in the near-infrared.

1. Introduction

NGC 6334 is a parsec long train of rich molecular clouds and HII regions located at galactic coordinates $l=351^\circ$, $b=0.^\circ7$. The complex lies at a distance of 1.74 kpc from the

¹Cerro Tololo Inter-American Observatory, National Optical Astronomy Observatory, Casilla 603, La Serena, Chile. CTIO is operated by AURA, Inc. under contract to the National Science Foundation.

²Visiting Astronomer, W.M. Keck Observatory

³Department of Astronomy, University of Florida, Gainesville, FL 32611

Sun (Neckel 1978), parallel to and located in the Carina-Sagittarius spiral arm. It is the site of possibly the largest number of recently formed OB stars observed in the Galaxy, which may have been triggered by the recent passage of a spiral density wave (Harvey & Gatley 1983).

NGC 6334 was first discovered in the far-infrared by Emerson, Jennings, & Moorwood (1973). Later observations in the far-infrared by McBreen et al. (1979), revealed six centers of emission. They were labeled by increasing southern declination using Roman numerals I-VI. Our observations were of NGC 6334 I, the northernmost far-infrared region of NGC 6334, and the site of a well-studied ultracompact HII region, NGC 6334 F. Though heavily obscured at visual wavelengths, NGC 6334 I is the center of a wealth of activity in the infrared, millimeter, and radio, as well as the site of many molecular sources and masers. Over the decades, many authors have studied this region of NGC 6334, and each, it seems, used nomenclature of their own to describe it. NGC 6334 I is a large region that is identified with several significant sources summarized by Kraemer et al. (1999). We will use the convention NGC 6334 F from the radio continuum observations of Rodríguez, Cantó, & Moran (1982) to describe the UCHII region we observed in the mid-infrared. The HII region is clearly cometary shaped in the radio (Rodríguez, Cantó, & Moran 1982; De Pree et al. 1995; Ellingsen, Norris, & McCulloch 1996), millimeter (Carral et al. 1997), and mid-infrared (De Buizer, Piña, & Telesco 2000; Persi et al. 1998), with its head pointing to the northwest and the tail running to the southeast. The peak of the UCHII region lies near the infrared source IRS-I 1 of Becklin & Neugebauer (1974), which has been presumed to be the ionizing source of the HII region. Harvey & Gatley (1983) also find another source $\sim 6''$ to the northwest of IRS-I 1, designated IRS-I 2, and yet another $\sim 18''$ to the east, designated IRS-I 3.

This region is very complex and is the site of a wide variety of activity. A near-infrared survey by Tapia, Persi, & Roth (1996) found an embedded young cluster of 93 sources associated with NGC 6334 I, all within a radius of $\sim 80''$. This cluster, of which IRS-I 1, IRS-I 2, and IRS-I 3 are members, appears to only contain stars earlier than B3-B4 according to Tapia, Persi, & Roth (1996). In light of the complexity of the NGC 6334 I area, interpretation of data is not an easy task. In this paper we present high-resolution mid-infrared images of the sources within NGC 6334 I. In §2 we will discuss the observations of NGC 6334 I, and explain the data reduction process in §3. Interpretation of our data and a discussion of the phenomenology of each source will be presented in §4. Finally, in §5 we will present our conclusions.

2. Instrumentation and Observations

Observations of NGC 6334 I were carried out in May of 1998 and 1999 on the Keck II 10-m telescope on Mauna Kea. Broadband N ($\lambda_o=10.46 \mu\text{m}$, $\Delta\lambda=5.1 \mu\text{m}$) and $IHW18$ (International Halley Watch, $\lambda_o=18.06 \mu\text{m}$, $\Delta\lambda=1.7 \mu\text{m}$) imaging was performed using OSCIR, the University of Florida mid-infrared camera/spectrometer. OSCIR is equipped with a 128×128 pixel, silicon/arsenic-doped blocked impurity band (Si:As BIB) array which is optimized for 8-25 μm work.

At Keck II, OSCIR has a field of view of $8''\times8''$, for a scale of $0''.0616 \text{ pixel}^{-1}$. Sky and telescopic radiative offsets were subtracted using a secondary chopping at 5 Hz, and by nodding the telescope every 15 seconds. Frame times of 15 ms were used for all observations. Images presented within this paper have total on-source integration times in both filters of 120 seconds for IRS-I 1, 480 seconds for IRS-I 2, and 240 seconds for IRS-I 3. The standard star α Boo was observed at roughly the same airmass (~ 1.7) as NGC 6334 I. It was used as a flux calibrator, with flux densities taken to be 683 Jy at N and 219 Jy at $IHW18$. Point-spread function (PSF) stars, were also imaged near the position of NGC 6334 I, yielding a measured full width at half maximum (FWHM) of $0''.33$ at N and $0''.41$ at $IHW18$.

3. Results and Data Reduction

We have observed NGC 6334 I previously as part of a mid-infrared survey using the Cerro Tololo Inter-American Observatory 4-m telescope (De Buizer, Piña, & Telesco 2000). The field of view at CTIO is large enough to encompass not only the UCHII region, but also the regions where IRS-I 2 and IRS-I 3 reside (Figure 1). We were able to image the whole central region of NGC 6334 I at both 10 and 18 μm , though the extended emission from IRS-I 3 is slightly off field in both filters. Because of the small field of view at Keck, we imaged the regions containing IRS-I 1, IRS-I 2, and IRS-I 3 individually (Figure 1). Carral et al. (1997) detect an additional source just southeast of IRS-I 2 at 7 mm. Not only was it not detected in the J , H , and K images of Persi et al. (1996), we did not detect it in our images from CTIO at either 10 or 18 μm (De Buizer, Piña, & Telesco 2000). Due to time constraints, we did not obtain follow-up images centered on this 7 mm source at Keck.

3.1. Flux Calibration

Because of the large bandwidth of the filters, the observed fluxes must be color corrected to account for the intrinsic source spectrum, the filter transmission, and the atmospheric

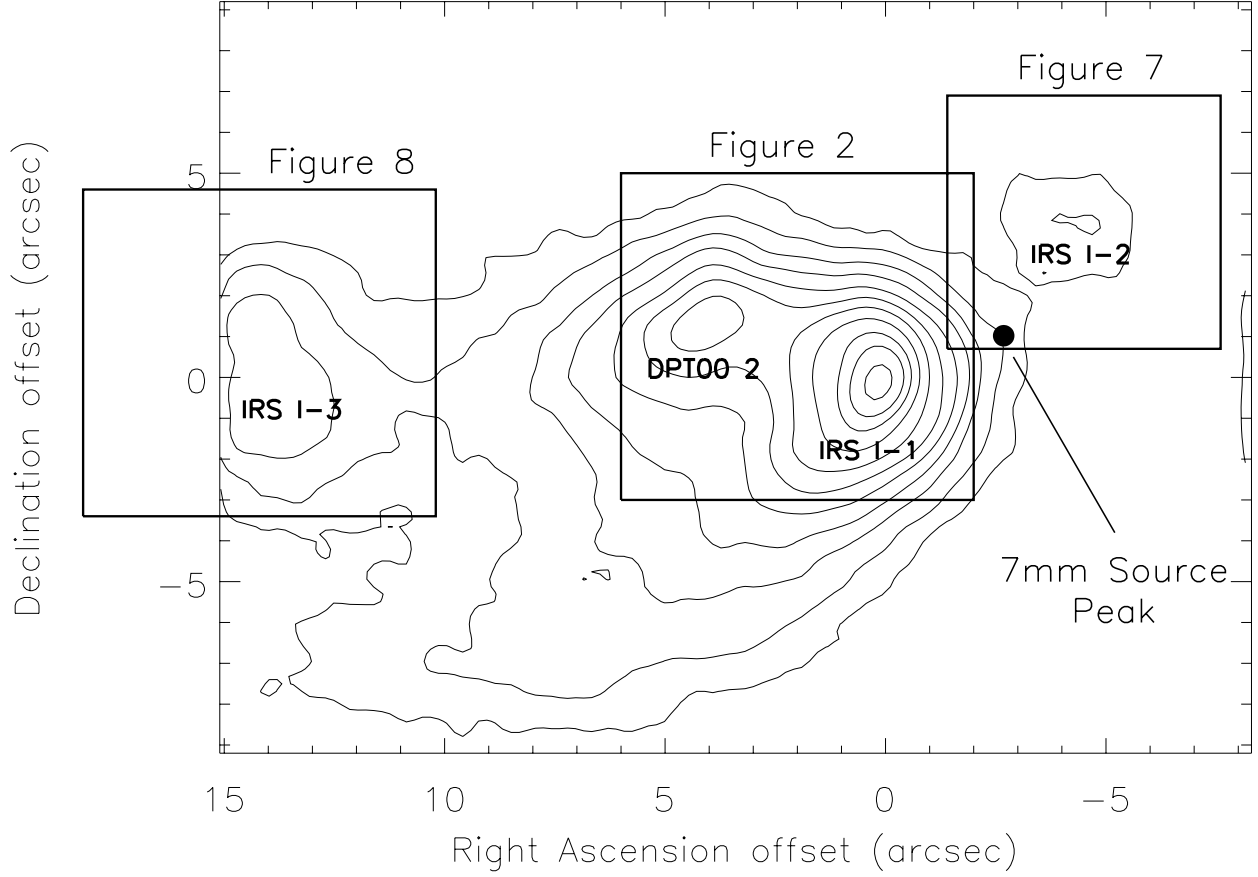


Fig. 1.— The central region of NGC 6334 I at $18\ \mu\text{m}$. This image was taken at the CTIO 4-m by De Buizer, Piña, & Telesco (2000) at a resolution of $\sim 1''$. The individual fields that were imaged at Keck are shown as boxes. At the center of this image is NGC 6334 F, a cometary UCHII region. It can be seen as two separate sources in the mid-infrared, IRS-I 1 and DPT00 2. Also labeled is the location of the 7 mm source seen by Carral et al. (1997). This source was not detected in our mid-infrared images. The coordinates of the origin are R.A.(J2000)= $17^{\text{h}}20^{\text{m}}53^{\text{s}}.44$ and Decl.(J2000)= $-35^{\circ}47'02''.2$.

transmission. For the calibration stars, the spectra were assumed to be a blackbody at the effective stellar temperature. Color corrected monochromatic flux densities, dust color temperatures, and optical depth values were obtained in a self-consistent manner by iteratively performing a numerical integration on the product of the Planck function, emissivity function (given by $1-e^{-\tau_\lambda}$, where τ_λ is given by the extinction law of Mathis 1990), filter transmission, solid angle subtended by the source, and model atmospheric transmission through the filter bandpass. A detailed treatment of this color-correction method is given in De Buizer (2000). As is often the case with mid-infrared observations, the calibration factor (ratio of accepted flux in Jy to analog-to-digital converter units per second per pixel) derived from the standard star observations changed throughout the course of the night due to changes in atmospheric conditions, but there was little correlation with airmass. Therefore, airmass corrections were not made to the observations. We can, however, estimate the absolute photometric accuracy (i.e. the mean calibration value of the standard star observations throughout the night divided by the standard deviation) associated with the tabulated color corrected flux densities in Table 1 to be 6.8% at 10 μm and 9.7% at 18 μm .

3.2. Temperature and Optical Depth Maps

One advantage of acquiring images at two wavelengths at Keck II is that we were able to construct dust color temperature (T) and emission optical depth (τ) maps for each source. This was accomplished by first convolving the 10 μm source images with the 18 μm image of a point-spread function (PSF) star, and the 18 μm source images with the 10 μm PSF image. This step is important because artificial structures in the temperature and optical depth maps can result from failure in having both images at the same resolution. This convolution process gives an effective resolution of the temperature and optical depth maps of $0''.53$. The relative alignment of the two images is also crucial to the values derived for temperature and optical depth. We employed an automated registration algorithm based on minimizing the sum of the squared residuals of the image difference as a function of the relative offsets. This algorithm generates a “chi-squared” surface at integral x and y pixel offsets. The chi-squared surface may then be interpolated to determine the location of the minimum to a hundredth of a pixel. Best-fit alignments for the image sets were found in this way for all sources.

Once an image set was spatially registered, the 10 and 18 μm flux densities for each pixel were used to iteratively solve for emission optical depth (τ) at 10 μm and dust color temperature under the assumption of blackbody emission. For these calculations we used the relationship $\tau_{10\mu\text{m}} = \tau_{18\mu\text{m}}/1.69$ from the extinction law of Mathis (1990). A cut-off

was applied to both the 10 and 18 μm flux density maps at 3σ above the background sky value. Temperature and optical depth values were only calculated for those areas that were above this cutoff at both wavelengths. The relative alignments of the 18 μm and 10 μm source images were then shifted by 4 pixels ($0''.25$) in various directions. It is unlikely that our registration of the images is off by such a large amount, however this allows a test of the robustness of the results concluded from the temperature and optical depth maps. It was found that these shifts significantly changed the peak temperature and optical depth values ($\pm 25\%$), however these shifts created only slight changes ($< 0''.3$) in the peak locations and overall morphologies. Therefore, while there may be uncertainty in the absolute values for these temperatures and optical depths, the maps are quite useful in demonstrating the spatial trends of these properties for these sources. The lower spatial scale color temperature and optical depth maps of Kraemer et al. (1999) look very similar to our maps, indicating that the structures in these maps are real.

3.3. Astrometry

Because of time constraints, careful astrometry was not performed. Therefore, accurate astrometry of the images needed to be performed by registering the mid-infrared images with other wavelength data. In the case of De Buizer, Piña, & Telesco (2000), the 5.0 cm radio continuum map of Caswell (1997) was registered with the mid-infrared images by aligning the radio and mid-infrared morphologies and peaks. Even with the higher spatial resolution images from Keck, it was found that the astrometry used in De Buizer, Piña, & Telesco (2000) does indeed show the best morphological coincidences between the mid-infrared images of NGC 6334 F and images at other wavelengths. We can not be completely sure that this is the correct astrometry because the morphologies may be wavelength dependent. However, this registration does show surprisingly good morphological coincidences throughout a broad range of wavelengths (6.2 cm, 5.0 cm, 3.5 cm, 2.0 cm, 1.3 cm, 2.2 μm), as we will discuss in more detail in §4.1. We therefore feel that the absolute astrometry of our mid-infrared sources is good to $\leq 0''.5$.

3.4. Luminosity and Spectral Type

Estimates of ZAMS stellar luminosities were made for each of the objects based upon their mid-infrared color-corrected fluxes. These are presented in Table 1. These values are based on the simplified assumption that all of the luminosity seen at the mid-infrared wavelengths is dust-reprocessed stellar radiation, and so is indicative of the true bolometric lu-

minosity of the stellar source itself. These mid-infrared luminosity estimates were computed by integrating the Planck function from 1 to 600 μm at the derived dust color temperature and optical depth for each source. This calculation employs the above emissivity function and assumes emission into 4π sr. Using the tables of Doyon (1990), which are based on the stellar atmospheric models of Kurucz (1979), we then found the ZAMS spectral types associated with those mid-infrared derived luminosities.

The main problems with this method of deriving estimates to the bolometric flux are 1) if the dust is anisotropically distributed around the source, the derived luminosity would depend on this dust distribution because some of the stellar flux will escape unprocessed through the unobstructed regions; 2) heavy obscuration could lead to non-negligible reprocessing by dust of the mid-infrared photons into far-infrared photons; 3) dust is in competition with gas for the short wavelength photons, which ionize the gas and produce UCHII regions. All of these processes would lead to underestimates of the bolometric luminosities from mid-infrared fluxes, however it is hard to quantify exactly how each contribute. For these reasons we believe that the derived bolometric luminosities represent good lower limit to the true bolometric luminosities.

As we will discuss later in the paper, some of these sources are believed not to be centrally heated. Therefore, the derived ZAMS spectral types in reality will not apply, and the luminosity given in Table 1 is a better indication of the infrared luminosity of the source, rather than the bolometric luminosity.

4. Discussion of Individual Sources

4.1. NGC 6334 F (IRS-I 1 and DPT00 2)

Mid-infrared observations of the UCHII region NGC 6334 F have revealed that it is composed of two sources (De Buizer, Piña, & Telesco 2000; Kraemer et al. 1999). Our brightest mid-infrared peak (Figure 2) is apparently the same as the peak of the cometary UCHII region seen in the radio maps of NGC 6334 F. Another mid-infrared source lies 4'' north-east of the mid-infrared peak, and is elongated in its thermal dust distribution. This source has been designated G351.42+0.64:DPT00 2 by De Buizer, Piña, & Telesco (2000), and is also referred to as NGC 6334:MFSW I:KDJ 4 from Kraemer et al. (1999). Throughout this paper we will refer to this source as DPT00 2 (Figure 1).

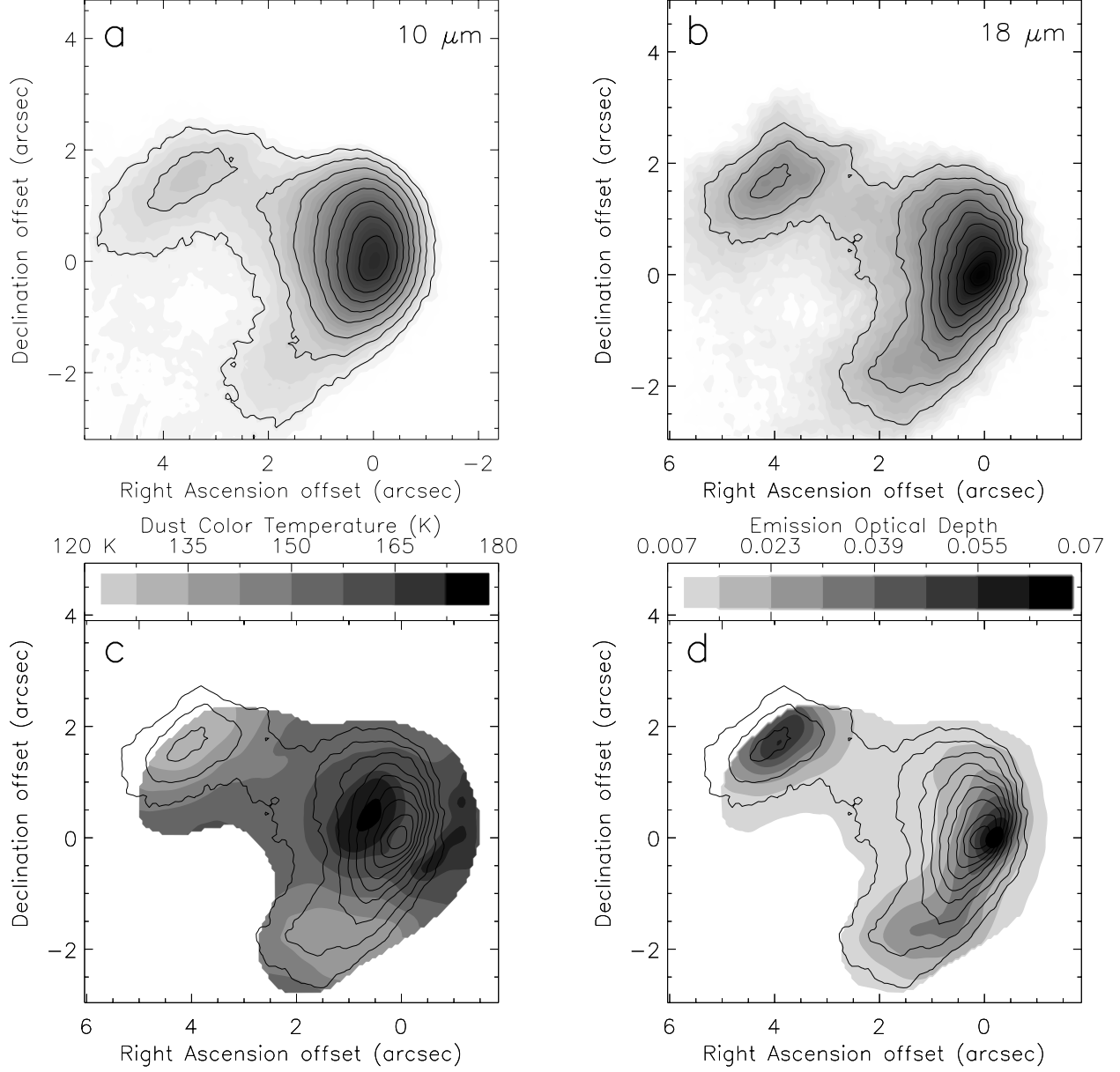


Fig. 2.— Keck data for NGC 6334 F. Panels a and b show the OSCIR images in grayscale at $10\ \mu\text{m}$ and $18\ \mu\text{m}$, respectively, convolved with a Gaussian kernel of FWHM 2 pixels. Contours are added for emphasis. In panel a, contour levels are 3, 4, 5, 6, 9, 12, 16, and $22\ \text{Jy arcsec}^{-2}$. In panel b, contour levels are 6.5, 10, 15, 20, 30, 40, 50, 60, and $80\ \text{Jy arcsec}^{-2}$. Panel c shows the color temperature map of the region, and panel d shows the emission optical depth map, both with the $18\ \mu\text{m}$ contours overlaid. The origin in each panel is the same as in Figure 1.

4.1.1. *Temperature and Optical Depth Maps*

In Figure 2d, one sees that the $18\ \mu\text{m}$ contours of IRS-I 1 delineate the optical depth contours (grayscale) fairly well. Looking at an overlay of the dust color temperature and the $18\ \mu\text{m}$ map (Figure 2c), the temperature peak is offset from the $18\ \mu\text{m}$ peak. Both of these observations indicate that the mid-infrared emission is bright there simply because it is optically thin in the mid-infrared and we are seeing through more material in the line of sight. This is a ridge of material that could have been swept up dust from the expanding shock front of the UCHII region. This leads to the conclusion that the mid-infrared peak may not be delineating the location of the exciting stellar source for the UCHII region.

4.1.2. *Radio Continuum*

The UCHII region of NGC6334F has been extensively observed at radio wavelengths. Due to similar spatial resolution ($\text{FWHM} \sim 0.5''$) and morphology, we used the 3.5 cm radio maps of Carral et al. (2002) to achieve accurate astrometry of our mid-infrared maps (Figure 3a). Using this astrometry, we also checked the mid-infrared morphology against other radio contour maps at similar resolution: the 5 cm ($\text{FWHM} \sim 2''$) of Caswell (1997), the 3.6 cm ($\text{FWHM} \sim 1.2''$) of Ellingsen, Norris, & McCulloch (1996), and the 2.0 cm map ($\text{FWHM} \sim 1.0''$) of De Pree et al. (1995) (Figure 3b). In all cases, the radio contours corresponded closely to those of the mid-infrared around the UCHII region peak, adding confidence to the idea that the radio and mid-infrared emission are coming from the same location. Comparing the radio maps with the mid-infrared images shows that radio emission comes not only from the location of the peak of the UCHII region, but from DPT00 2 as well. The radio continuum emission seems to trace the southern edge of DPT00 2 where it faces the peak of the UCHII region, indicating that it may be externally ionized. The color temperature maps are consistent with this scenario. The southern edge of DPT00 2 is also the hottest part of the source, and therefore may not be internally heated (Figure 2c).

4.1.3. *Comparisons to the Observations of Harvey and Gatley (1983)*

The peak in the UCHII region at $18\ \mu\text{m}$ apparently corresponds to the IRS-I 1 peak of Harvey & Gatley (1983). Overlays between our $18\ \mu\text{m}$ mid-infrared maps and the $20\ \mu\text{m}$ mid-infrared maps of Harvey & Gatley (1983) show similar morphology with two peaks with the same separations as IRS-I 1 and IRS-I 2 (Figure 4a). The $20\ \mu\text{m}$ maps of Harvey & Gatley (1983) show extension in the direction of DPT00 2, but do not resolve the source.

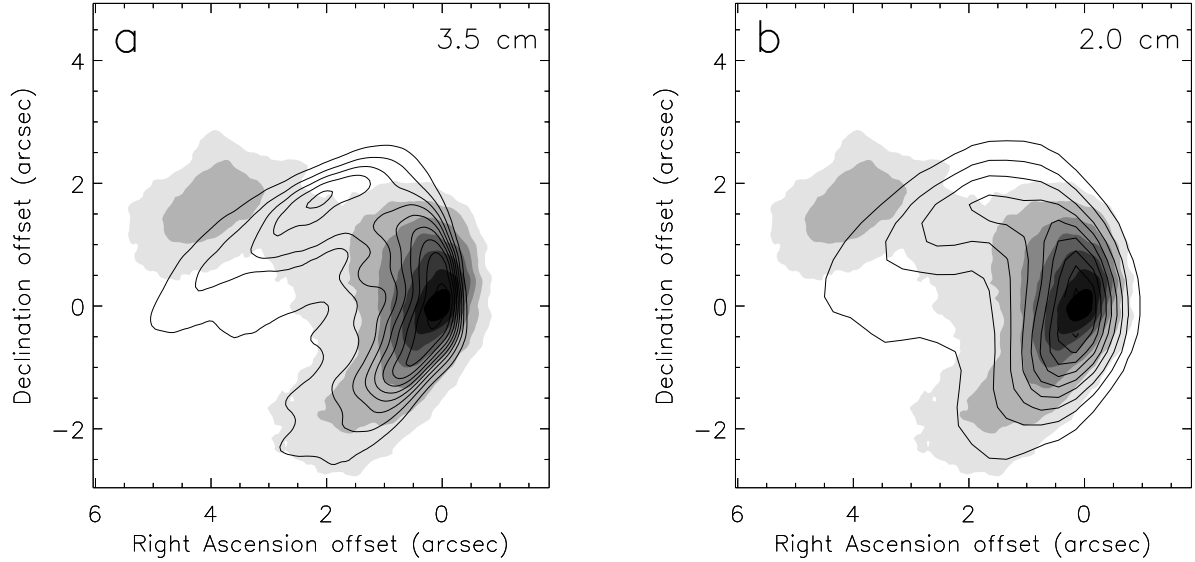


Fig. 3.— Comparisons of the $18\ \mu\text{m}$ images (filled contours) with radio continuum images (contours) demonstrate that the contours of the radio continuum and mid-infrared are correlated for IRS-I 1. Panel a shows the 3.5 cm radio continuum images of Carral et al. (2002) registered with respect to the mid-infrared image. By registering the mid-infrared images with respect to the radio continuum images, the mid-infrared absolute astrometry was determined. Panel b shows the registration between the 2.0 cm maps of De Pree et al. (1996) and the mid-infrared. The origin in both panels is the same as in Figure 1.

Using the astrometry above, we find that the absolute coordinates of the $20\ \mu\text{m}$ peaks of IRS-I 1 and IRS-I 2 from Harvey & Gatley (1983) are both in error by approximately $1''.5$ in the southern direction. This is entirely plausible, given that these observations were performed by scanning the area with a photometer with a $4''$ beam, though the quoted positional accuracy is $1''$. Assuming our astrometry is correct and using the coordinates of the peak of the radio continuum from Carral et al. (2002), the mid-infrared peak of IRS-I 1 is at R.A.(J2000)= $17^h20^m53^s.44$, Decl.(J2000)= $-35^\circ47'02''.16$. This changes the mid-infrared coordinates for the other sources as well. These new coordinates are given in Table 1.

4.1.4. Ammonia Distribution

Ammonia observations by Kraemer and Jackson (1995) show the UCHII region to be bounded by ammonia (3,3) emission to the west. This emission is a dense gas indicator, as is CS $7\rightarrow6$ which also peaks west of the UCHII region (Kraemer et al. 1999). It appears therefore that the star responsible for ionizing the UCHII region exists on the edge of this density enhancement, and this gradient in the surrounding medium is what has led to the shape of the UCHII region. These observations seem to indicate the cometary appearance is due to a champagne-like flow, rather than a bow-shock caused by supersonic motion through the interstellar medium.

In Figure 7 of Kraemer et al. (1999), they show an overlay of their mid-infrared and ammonia observations by registering them using the coordinates of Harvey & Gatley (1983), which we believe to be in error. We present in Figure 4b the correctly registered integrated ammonia map of Kraemer et al. (1999) and our mid-infrared map of the region. Because the radio continuum and ammonia maps were taken at the same time, they have extremely accurate relative astrometry. We overplotted the integrated ammonia in Figure 4b by first registering the radio continuum peak of Kraemer et al. (1999) with our mid-infrared peak for IRS-I 1. The integrated ammonia map presented in Figure 4b is mostly ammonia emission but also contains ammonia seen in absorption. The weakest contour of ammonia in the integrated map appears to wrap around the mid-infrared peak in Figure 4b. This ammonia component is associated with the mid-infrared (and radio continuum) peak and is actually seen in absorption by Kraemer and Jackson (1995). The rest of the integrated map shows ammonia emission, bounded by IRS-I 1 to the east and IRS-I 2 lies just to the west of the secondary peak. The ammonia emission follows along the eastern edge of the UCHII region, extending to the south.

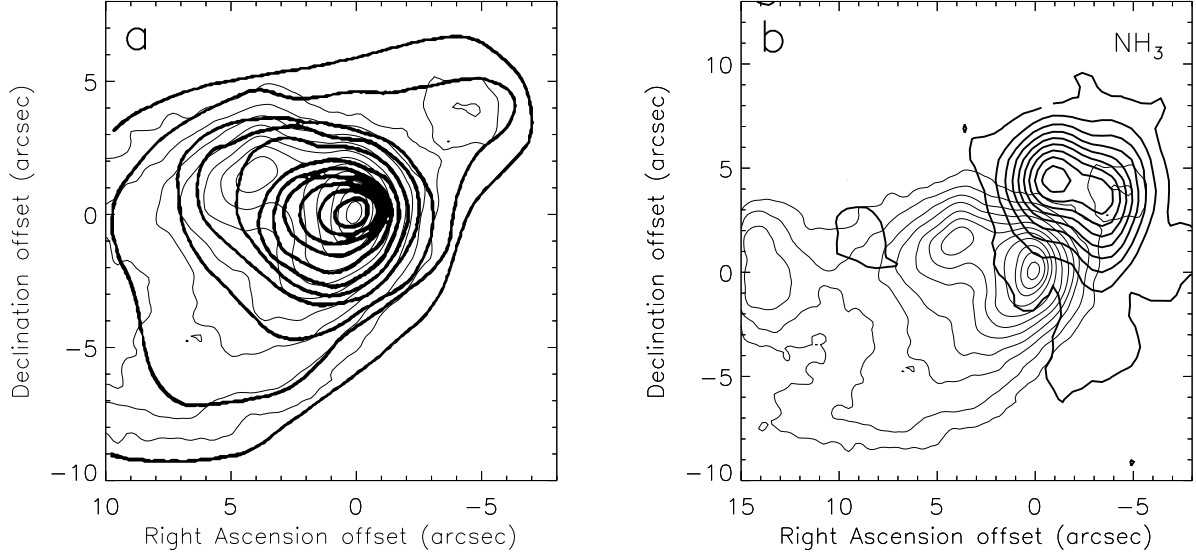


Fig. 4.— Comparisons of the 18 μm emission from NGC 6334 I with other large-scale emission. Panel a shows the 20 μm contours (thick) of Harvey and Gatley (1983) compared to the 18 μm contours (thin) from De Buizer, Piña, & Telesco (2000). A very good match is found, leading us to a revision in the mid-infrared coordinates of Harvey and Gatley (1983). Panel b shows the integrated ammonia map (thick contours) of Kraemer et al. (1999) registered with respect to the mid-infrared images from De Buizer, Piña, & Telesco (2000, thin contours) using the new mid-infrared coordinates. The ammonia appears to bound the UCHII region on to the west, and may be responsible for the champagne-like flow manifesting itself as the cometary shaped UCHII region. The origin in both panels is the same as in Figure 1.

4.1.5. *Masers*

The maser emission in this region is concentrated near IRS-I 1 (Figure 5). This area is marked by several molecular maser species: methanol (Ellingsen et al. 1996), water (Forster & Caswell 1989), and hydroxyl (Gaume & Mutel 1987). A majority of the masers seem to be on the sharp western edge of the UCHII region which is bounded by the ammonia emission (Figures 5a and 5b). This density enhanced side of the UCHII region will also be a location where the expansion of the ionized material will first impact as a shock front. The density and energetics of such a region would be suitable for creating and sustaining maser emission. If this is the case, the masers that exist on this sharp boundary may be shock-induced.

There is a long string of water masers that are offset to the north of the mid-infrared emission from the IRS-I 1. Strings of water masers can be interpreted as coming from and delineating outflow (e.g. Claussen et al. 1997). However, water masers are also known to exist coincident with “hot cores” as seen from their molecular emission (Cesaroni et al. 1994). Observations of G9.62-0.19 (Hofner & Churchwell 1996) show a string of water masers emanating radially from a UCHII region center. However, the ammonia observations of Cesaroni et al. (1994) show a peak at the same position as the water masers, and it has been proposed that these water masers are delineating the location of a hot core. Likewise, given the corrected astrometry set forth in this paper, the primary ammonia peak north of IRS-I 1 is coincident with the water maser string. It is plausible that these water masers are delineating the site of a hot core.

There is also a group of methanol masers that are offset northwest of IRS-I 1, that are thought to be associated with IRS-I 2 (Figure 5c). Our astrometry shows that they are not exactly coincident with this mid-infrared source, and are close to the secondary ammonia peak (Figure 5a). These methanol masers may be delineating a second hot core in the ammonia. Both of these maser strings may delineate the location of hot cores that are too cool and/or embedded to see in the thermal infrared.

4.1.6. *Mid- Infrared versus Near Infrared Sources*

Persi et al. (1996) observed this area in the near infrared bands J($1.25\ \mu\text{m}$), H($1.65\ \mu\text{m}$) and K($2.2\ \mu\text{m}$) at a resolution of $0''.9$. These observations revealed 4 sources within $3''$ of the IRS-I 1 peak. The near infrared sources are labelled IRS1E, IRS1W, IRS1SE, and IRS1SW (Figure 6). These sources are highly reddened and therefore believed not to be foreground stars. Persi et al. (1996) claims that the IRS1E source is coincident with the $30\ \mu\text{m}$ peak of Harvey & Gatley (1983). Overlaying the K image with our mid-infrared images shows good

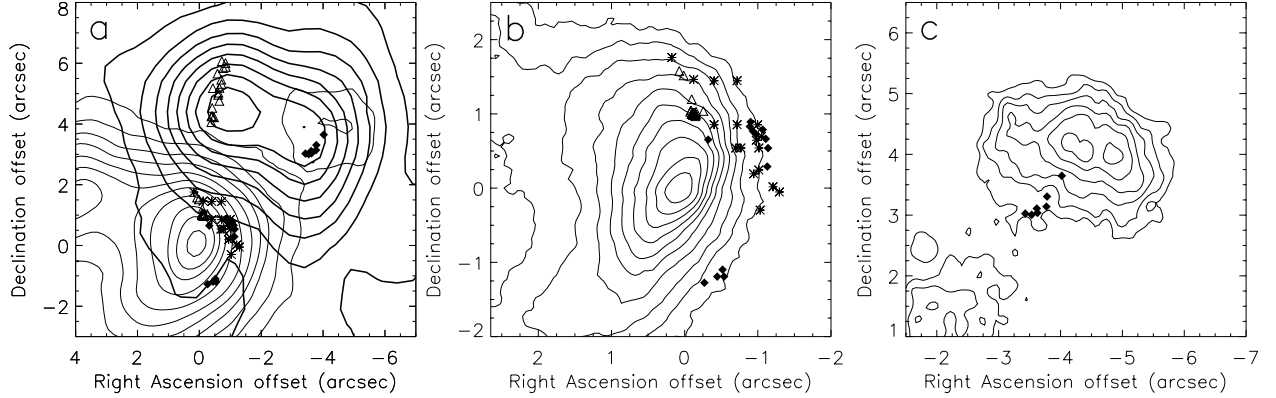


Fig. 5.— The water (triangles), hydroxyl (stars), and methanol (filled diamonds) masers in the NGC 6334 I region. Panel a shows that a majority of the masers are associated with the sharp boundary between the 18 μm emission (thin contours) of IRS-I 1 and the ammonia emission (thick contours). This 18 μm image is from the CTIO 4-m (De Buizer, Piña, & Telesco 2000). A string of water masers may be associated with the brightest peak of the ammonia distribution, and a string of methanol masers may be associated with the secondary peak. Panel b zooms in closer to IRS-I 1 to show that the masers are all excited along the sharp western edge of the source. Panel c shows that the methanol masers that were thought to be associated with IRS-I 2 are not coincident with the mid-infrared source peak. The origin in each panel is the same as in Figure 1.

morphological coincidences with both IRS-I 1 and IRS-I 3 (see §4.3), leading us to believe the relative astrometry between the near-infrared and mid-infrared to be better than $0''.5$. This alignment places IRS1E peak approximately $1''.8$ from the $30\ \mu\text{m}$ peak and $0''.7$ from our $18\ \mu\text{m}$ peak.

Overlaying the K band image with the color temperature map generated from our mid-infrared images we see a very important coincidence that once again leads us to believe our astrometry is correct (Figure 6d). The color temperature is peaked near the location of a near infrared source (IRS1E). Also, there is a near infrared source seen at J and H, and extended at K, coincident with the south-eastern portion of DPT00 2 (Figure 6c). We see in the temperature map in Figure 6d that the hottest parts of DPT00 2 are on the side facing the UCHII region. Since this region is hotter, it should be more readily seen in the near infrared. These coincidences of the hotter regions to near infrared emission seem to confirm our relative astrometry. The coincidence of IRS1E to the peak in the color temperature map also leads us to speculate that the near infrared source IRS1E may be responsible for the central heating and ionizing of the the UCHII region.

The nature of IRS1W and IRS1SW can also be speculated from the color temperature and optical depth maps. By looking at the near-infrared images of Persi et al. (1996) in Figure 6, we see that as one views this region at shorter and shorter wavelengths the near-emission comes only from the sources within the mid-infrared arc of emission from IRS-I 1. Since the optical depth is largest at the mid-infrared peak, this is where there is a higher concentration of cooler material. At J and H, IRS1W and IRS1SW lie just north and just south of the mid-infrared peak (Figures 6a and 6b). The near-infrared emission is coming from areas where thermal dust emission is located, but not at its densest and brightest parts. Furthermore, both of these sources are not temperature peaks in the color temperature map (Figure 6d). If IRS1W and IRS1SW are not hot, there must be an alternate reason why they are visible in the near infrared.

One scenario is that IRS1W and IRS1SW are visible in the near-infrared because of shock excited emission (De Buizer 2002). These sources are most prominent at J and H, and both of these filter bandpasses encompass many lines of [FeII]. These spectral lines are shock indicators (McKee, Chernoff, and Hollenbach 1984), two of the strongest being the lines at 1.26 and $1.64\ \mu\text{m}$ (roughly the central wavelengths of the J and H filters). Bloomer et al. (1998) observed a diffuse UCHII region like NGC 6334 F and find that the thermal dust emission and narrow line [FeII] images are well matched spatially. As discussed above, the shape of the UCHII region and the presence of masers on the sharp western boundary imply that the masers may be shock excited. In this same location there is a density enhancement of dust, as seen in the mid-infrared, which may be swept up material from an expanding shock

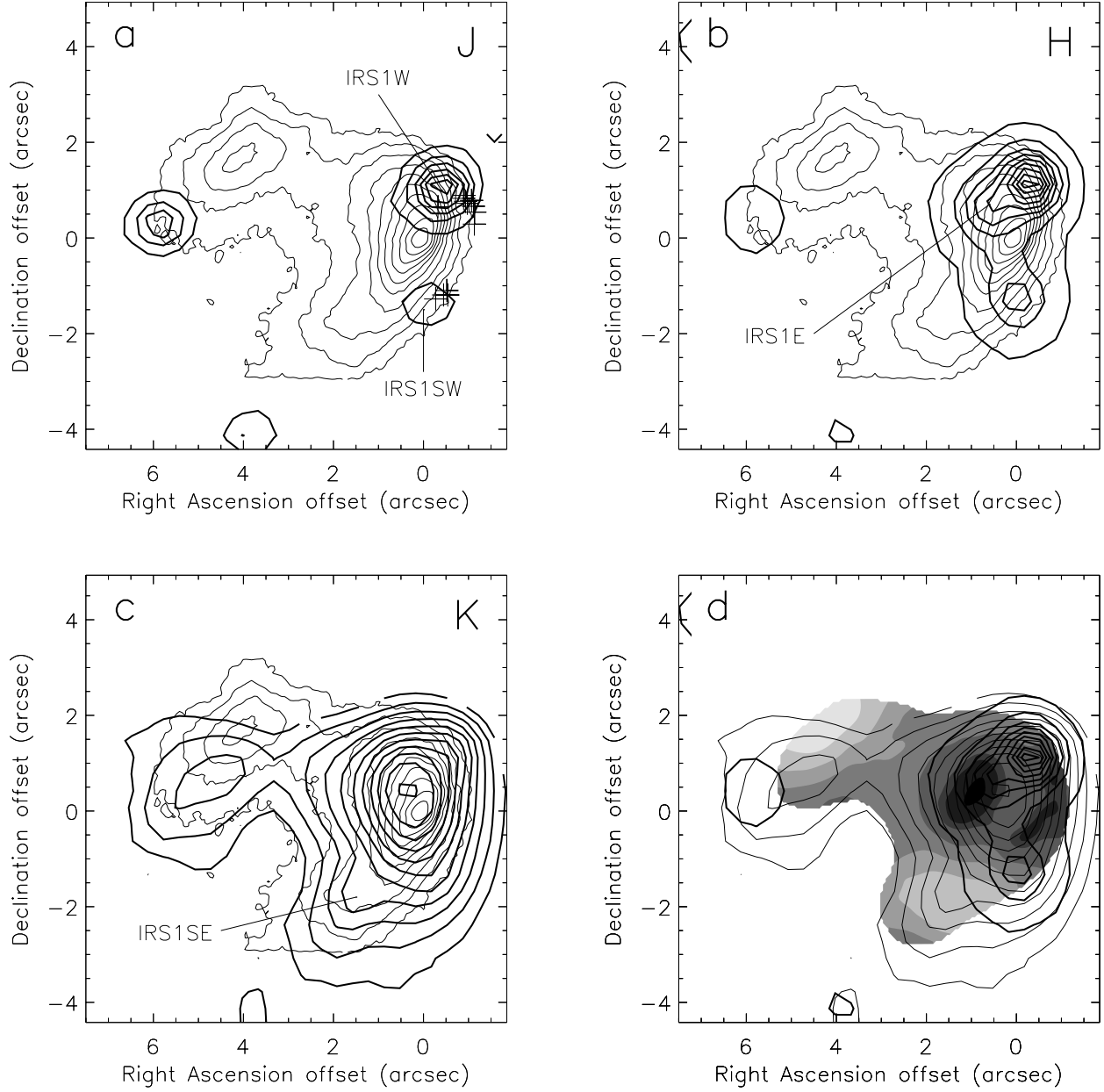


Fig. 6.— The near infrared sources in the region near IRS-I 1 from Persi et al. (1996). Panel a, b and c, show the near-infrared (thick contours) J, H, and K images, respectively, overplotting the 18 μm Keck contours (thin). Labels are the names of the near-infrared sources given by Persi et al. (1996). The methanol masers are plotted in panel a as crosses. They appear to be associated with two near infrared sources. Panel d shows the color temperature map (filled contours) overlaid with the K emission (thin contours) and H emission (thick contours). The origin in each panel is the same as in Figure 1.

front rather than circumstellar in origin. IRS1W is located on this dust ridge and coincident with the majority of the masers here and is most prominent in the J and H bands, which contain several lines that are shock indicators. For all of these reasons, it seems plausible that IRS1W and IRS1SW are not stellar sources themselves, but instead may be areas of shock excited emission. The final proof of such a hypothesis would be to obtain near-infrared spectra of these sources.

However, inconsistent this scenario is the near-infrared H_2 observation shown in the article by Persi et al. (1996) that does not seem to show any shock-excited H_2 emission at these locations. Greenhouse et al. (1991) finds that H_2 emission (a more widely used shock indicator) and [FeII] are well correlated in their emission. Therefore, an alternative scenario could be that IRS1W and IRS1SW are simply areas of reflected emission from the less-extinguished parts of IRS-I 1.

As for the near-infrared source IRS1SE, we see no mid-infrared source or peak at this location, but it is an area of diffuse mid-infrared emission. It seems that IRS1SE is not a stellar source either, and that the near-infrared emission may likely be coming from reflected or scattered photons off of the tail of the UCHII region.

4.2. IRS-I 2

The Keck images of IRS-I 2 reveal it to be an elongated and low-surface brightness source. The source is relatively low signal-to-noise (peak pixel $S/N \sim 7$), but smoothing (3 pixel gaussian) shows three peaks in the thermal emission along the direction of elongation (Figure 7). The central and western peaks are comparable in brightness, however the eastern source is fainter, especially at $18 \mu m$. Because the western peak can be clearly seen at both 10 and $18 \mu m$, we chose this location as the reference position for IRS-I 2 in Figure 7, and give the coordinates for this location in Table 1. Overlays of the NGC 6334 I region from Harvey & Gatley (1983) and our $18 \mu m$ data show a good match in the peak locations, confirming that the source seen at Keck is indeed IRS-I 2 (Figure 4a).

The source elongation in the mid-infrared is at a position angle of $\sim 65^\circ$. The methanol masers near this source (Ellingsen et al. 1996) lie at an angle of approximately -35° , almost perpendicular to the thermal dust elongation (Figure 5c). However, the masers are not coincident with IRS-I 2. The measured distance from the center of the maser distribution to the center of brightness in the $18 \mu m$ emission from IRS-I 2 is $1.25''$. Again, these masers lie close to the secondary peak in the thermal ammonia emission, and may be delineating the sight of a second hot core or embedded protostar, instead of being associated directly with

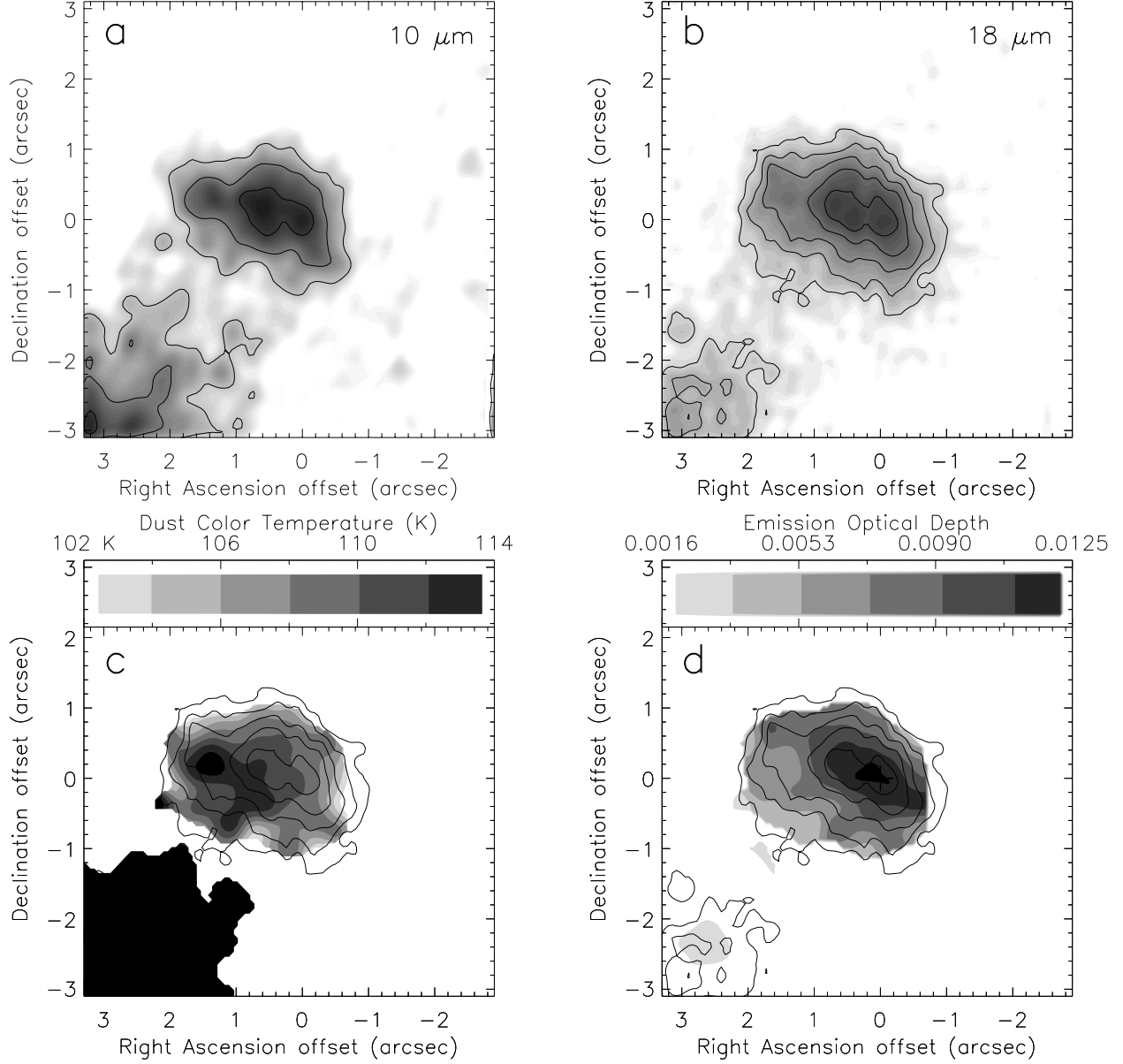


Fig. 7.— Keck data for IRS-I 2. Panels a and b show the OSCIR images in grayscale at 10 and $18\ \mu\text{m}$, respectively, convolved with a Gaussian kernel of FWHM 3 pixels. Contours are added for emphasis. In panel a, contour levels are 15, 40, and $60\ \text{mJy arcsec}^{-2}$. In panel b, contour levels are 200, 400, 600, 800, and $1000\ \text{mJy arcsec}^{-2}$. Panel c shows the color temperature map of the region, and panel d shows the emission optical depth map, both with the $18\ \mu\text{m}$ contours overlaid. The origin in each panel is $\text{R.A. (J2000)} = 17^{\text{h}}20^{\text{m}}53^{\text{s}}.04$ and $\text{Decl. (J2000)} = -35^{\circ}46'58''.3$.

the IRS-I 2.

Looking to the color temperature maps of this source show that the hottest part of the source is the eastern peak (Figure 7c). By overlaying the optical depth maps with the $18\ \mu\text{m}$ contours, one can see that the optical depth distribution for the central and western sources trace the $18\ \mu\text{m}$ contours well (Figure 7d). This implies that these two sources are bright merely because we are seeing through more optically thin mid-infrared emitting material. As in the case for IRS-I 1, it may be likely that the stellar heating source does not lie at the mid-infrared peak and that the temperature peak may be the location of the stellar source. However, there are two reasons this argument may not be applicable in this instance. First, unlike IRS-I 1, we cannot be sure that the temperature peak is the location of the stellar source because there is no near-infrared component at this location (Persi et al. 1996). If it is hotter we would expect the energy distribution to rise towards the near infrared, in the absence of significant extinction. This leads to a second point, which is that the temperature “peak” in this case is only 12 K hotter than the coolest parts of the source. This is unlike IRS-I 1, where the temperature peak is diffinitive because it is twice as hot ($\Delta T = 60\ \text{K}$) as the coolest areas mapped. Given the fact that the source is relatively flat both in mid-infrared flux and color temperature, IRS-I 2 may not be internally heated. Because the temperature map shows this source to be warmest on the side facing the ammonia peak, if there is an embedded stellar or proto-stellar source at this location, it may be responsible for this slight heating of IRS-I 2. This side of the molecular core would have to have less extinction than the side facing the earth, allowing heating of IRS-I 2 without a direct view of the heating source from the earth.

There is mid-infrared emission in the southeast corner of the images of IRS-I 2 from Keck (Figure 7a). This emission is located approximately where we would expect the 7 mm source of Carral et al. (1997) to be located. However, the emission is diffuse and cut off by the edge of the array. It is most likely just extended emission from IRS-I 1. The most recent high sensitivity study of this source was performed by Carral et al. (2002) and does not confirm the detection of this source at 7 mm. They claim that the source seen in their previous 7 mm study may have been an artifact of the data reduction and the limited (u,v) coverage of the observations.

4.3. IRS-I 3

This source has low surface brightness and is hour-glass shaped in the mid-infrared, however the northern lobe of the source is more extended in the northern direction at $10\ \mu\text{m}$ than at $18\ \mu\text{m}$ (Figures 8a and 8b). Kraemer et al. (1999) claim that the emission drops by

$\sim 20\%$ in the area between the peaks at $20\ \mu\text{m}$. Our higher resolution images show emission drops by almost 80% at $18\ \mu\text{m}$ and 70% at $10\ \mu\text{m}$ between the peaks, so that the sources appear as separate objects in the mid-infrared. Kraemer et al. (1999) speculate that this source may derive its double-lobed shape because it is a torus or dust disk around a central star. This seems unlikely given that the higher resolution images show elongation in the lobes perpendicular to the plane of the speculated disk.

The near infrared images of Persi et al. (1996) from this area show that the mid-infrared emission of IRS-I 3 is coming from a cluster of (~ 7) near-infrared sources with extended emission in H (Figure 9) and K. The overall extended shape of the near-infrared emission compared to that in the mid-infrared again strengthens our belief that the relative astrometry between the near-infrared and mid-infrared for all these NGC 6334 I sources is accurate. The brightest source coincident with IRS-I 3 in the H band image of Persi et al. (1996) appears to be located near the central temperature peak (Figure 9b). This bright near-infrared star, which is also seen at J and K, may be responsible for the central ionizing and heating the IRS-I 3. Another near-infrared source is located just northeast of the northern lobe. This is the location of the temperature maximum in the color temperature maps, and therefore this star may be externally heating this part of the mid-infrared source.

Overlaying the $20\ \mu\text{m}$ image from Harvey & Gatley (1983) with our $18\ \mu\text{m}$ image does show good coincidence between the peaks of IRS-I 1 and IRS-I 3. However, the coordinates quoted for this source from Harvey & Gatley (1983) are actually from the $2.2\ \mu\text{m}$ observations of Becklin & Neugebauer (1974). This position is offset from the position of the mid-infrared source we observe and the near-infrared emission of Persi et al. (1996) (Figure 9). The most likely reason for this difference in position is because the images of Becklin & Neugebauer (1974) were taken with scans from a near-infrared photometer with an effective beam size of $\sim 8''$. The offset between the brightest near-infrared source and the position quoted by Becklin & Neugebauer (1974) is $3''.4$ in right ascension and $1''.4$ in declination, well within the errors they quote of $5''$ for right ascension and $4''$ for declination.

Because the morphologies and peaks of IRS-I 3 are different at 10 and $18\ \mu\text{m}$, and because of the extremely extended nature of the mid-infrared emission, it is difficult to assign reference coordinates to the source. In Figure 8 we arbitrarily show the $10\ \mu\text{m}$ peak in the southern lobe of IRS-I 3 as the reference position. Coordinates for this position are given in Table 1.

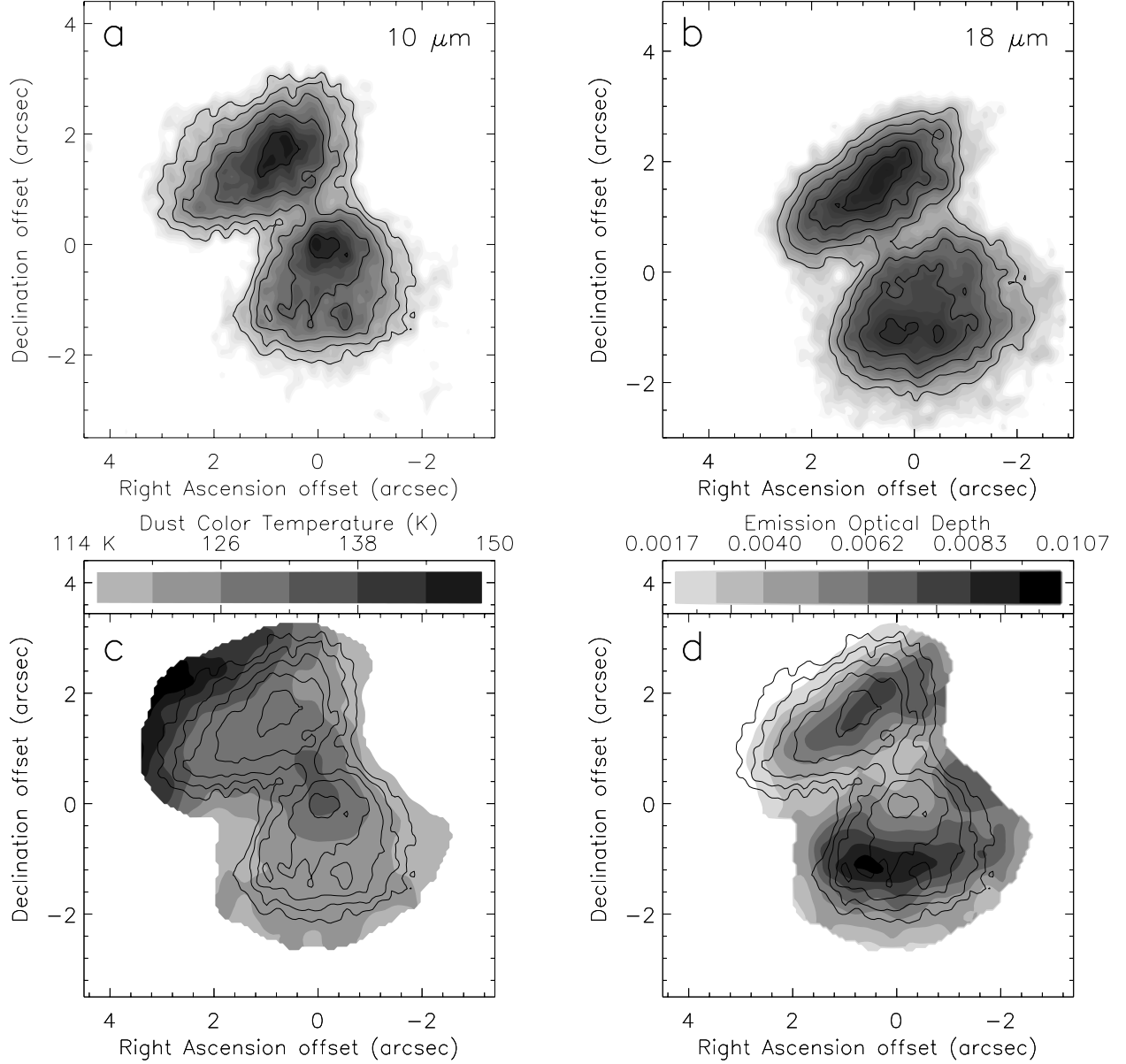


Fig. 8.— Keck data for IRS-I 3. Panels a and b show the OSCIR images in grayscale at 10 and 18 μm , respectively, convolved with a Gaussian kernel of FWHM 3 pixels. Contours are added for emphasis. In panel a, contour levels are 65, 85, 110, 150, and 200 mJy arcsec^{-2} . In panel b, contour levels are 600, 800, 1000, 1250, and 1600 mJy arcsec^{-2} . Panel c shows the color temperature map of the region, and panel d shows the emission optical depth map, both with the 18 μm contours overlaid. The origin in each panel is $\text{R.A. (J2000)} = 17^{\text{h}}20^{\text{m}}54^{\text{s}}.60$ and $\text{Decl. (J2000)} = -35^{\circ}47'02''.6$. The apparent offset between panel a and b is not real, and simply a change in the position of the origin in the panels.

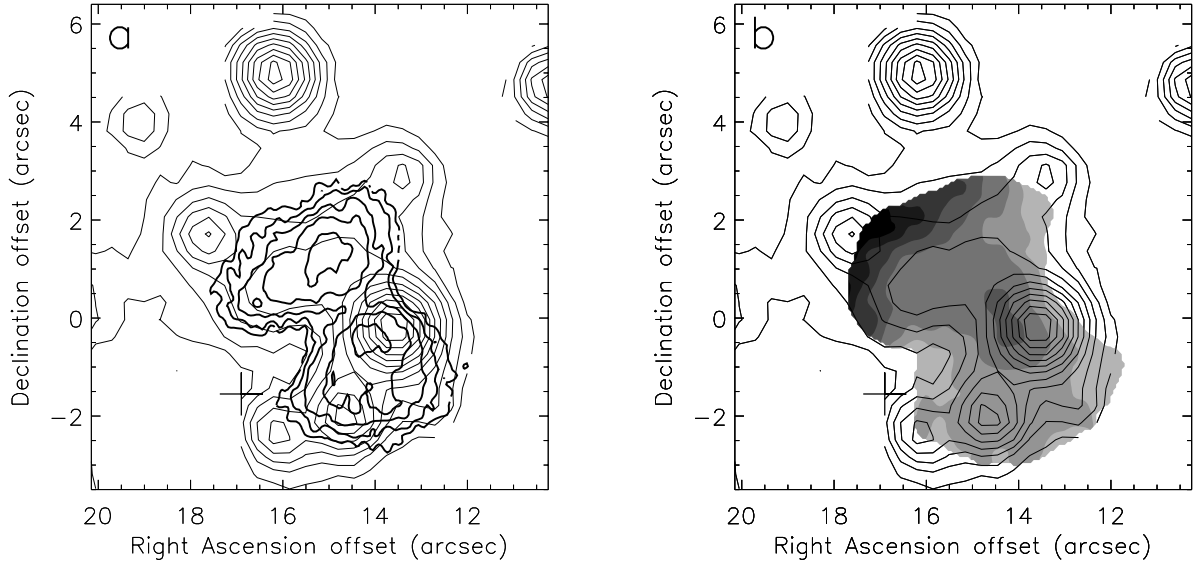


Fig. 9.— A cluster of near infrared sources coincident with IRS-I 3. Panel a shows the H band (thin contours), overlaid on the Keck 10 μm extended emission (thick contours). Panel b shows the H band overlaid on the color temperature map for IRS-I 3 (filled contours). The low-spatial resolution ($\sim 8''$) 2.2 μm peak of Becklin and Neugebauer (1974) for IRS-I 3 is plotted here as a cross. This obvious discrepancy in position has lead us to a revision in the mid-infrared coordinates of IRS-I 3. The origin in both panels is the same as in Figure 1.

5. Conclusions

High resolution mid-infrared observations of the central region of NGC 6334 I have revealed much about the nature and properties of the sources there. The UCHII region NGC 6334 F is composed of two sources, IRS-I 1 and G351.42+0.64:DPT00 2. The peak of IRS-I 1 appears to be coincident with the peak in the radio continuum. Ammonia observations of Kraemer et al. (1999) when registered properly with our mid-infrared data indicate that the shape of the UCHII region is not due to a bow-shock, but instead due to champagne-like flow from stellar source at the edge of a molecular clump. Maser emission is concentrated at this interface between the mid-infrared and ammonia emission, and may therefore be shock induced. There are two other strings of masers that lie near the two peaks in the ammonia emission and may be delineating the sites of hot molecular cores that are too young and/or embedded to be seen yet in the mid-infrared.

The mid-infrared emission from IRS-I 1 seems to be coming from an arc of dust at the interface between the molecular ammonia clump and the UCHII region, and may be material swept up by the expanding shock front of the UCHII region. The color temperature peaks at a location interior to this mid-infrared arc, coincident with a near infrared source IRS1E. This source may be the stellar source responsible for the ionization and heating of the NGC 6334 F region. Two other near infrared sources, IRS1W and IRS1SW, lie in the northern and southern parts of the mid-infrared arc and are associated with the majority of the masers in the region. There is no temperature peak at these locations, so the near infrared emission may just be reflected or shock excited emission. A fourth near infrared source (IRS1SE) seems to simply be reflected emission off the UCHII region tail.

G351.42+0.64:DPT00 2 appears to be a clump of dust, perhaps swept up by the shock front of UCHII region. It displays a steep temperature gradient towards the color temperature peak. It also shows some signs of ionized emission in the higher resolution radio continuum images, but only on the hotter, southern side. For these reasons it may be that DPT00 2 has no central heating source but is simply heated and ionized by the same source heating and ionizing IRS-I 1 (IRS1E) .

IRS-I 2 was believed to be associated with the a linear structure of methanol masers and perhaps delineating a circumstellar disk. However, the thermal dust emission is elongated at a different position angle to the position angle of the maser distribution. The low-surface brightness, smooth color temperature distribution, and lack of a near-infrared component may indicate that there is no internal stellar source here at all. Furthermore, the masers are offset from the mid-infrared peak and could be associated with the secondary peak in the ammonia distribution.

Lower resolution mid-infrared images of IRS-I 3 showed it to be a double peaked source. However, the high resolution images presented here show that it has a complex and peculiar morphology. We find, using the near infrared data of Persi et al. (1996), that the large and extended mid-infrared sources are extended dust emission from a cluster of stellar sources seen in the near infrared. These stellar sources have directly influenced the morphology in the mid-infrared, and the structure of the source as seen in the color temperature map.

The reality of the 7 mm source in this region has been seriously called into question by the non-detection in the mid-infrared, and has recently been discovered to be an artifact of data reduction by follow-up observations of the original authors.

The authors would like to thank NASA’s Florida Space Grant Consortium for their financial support of the first author at the time of observations. Data presented herein were obtained at the W.M. Keck Observatory, which is operated as a scientific partnership among the California Institute of Technology, the University of California and the National Aeronautics and Space Administration. The Observatory was made possible by the generous financial support of the W.M. Keck Foundation. The authors wish to recognize and acknowledge the very significant cultural role and reverence that the summit of Mauna Kea has always had within the indigenous Hawaiian community. We are most fortunate to have the opportunity to conduct observations from this mountain.

Table 1. Properties of Sources in NGC 6444 I

Source	10 μm Flux Density [†] (Jy)	18 μm Flux Density [†] (Jy)	Offset [‡] ($\Delta\alpha$, $\Delta\delta$) (arcsec)	Right Ascension [‡] (J2000)	Declination [‡] (J2000)	Lum
IRS-I 1	78.63 \pm 5.42	222.70 \pm 21.60	(0,0)	17 20 53.44	-35 47 02.2	
IRS-I 2 [‡]	0.13 \pm 0.01	3.41 \pm 0.33	(-4.8,+3.9)	17 20 53.04	-35 46 58.3	
IRS-I 3 (all)	2.22 \pm 0.15	22.96 \pm 2.23	(+14.1,-0.4)	17 20 54.60	-35 47 02.6	
...north lobe	1.09 \pm 0.07	8.57 \pm 0.83	
...south lobe	1.24 \pm 0.08	12.87 \pm 1.25	
DPT00 2	11.37 \pm 0.77	68.65 \pm 6.66	(+4.0,+1.6)	17 20 53.77	-35 47 00.6	

[†]Color corrected flux densities. The quoted errors in the measurements are the absolute photometric a (dominant source of error), which was calculated to be 6.8% at 10 μm and 9.7% at 18 μm . All extended sources were included for all sources, and may lead to the small differences between the values quoted here and that of De Buizer et al. (2000) .

[‡]Refer to the text and Figures 7 and 8 for locations of these coordinates for the extended sources IRS-I 1, 2, and 3.

*Luminosities and spectral types are given for all objects for the sake of completeness. Some sources may have multiple cores, or may be heated by more than one star (see text).

[‡]Flux densities for IRS-I 2 are much different than those quoted in De Buizer, Piña, & Telesco (2000). This is due to the fact that the CTIO 4-m images yielded very low signal-to-noise for IRS-I 2.

REFERENCES

- Becklin, E.E., & Neugebauer, G. 1974, in ESRO Symp.105, HII regions and the Galactic Center, ed. A.F.M. Moorwood (Noordwijk, The Netherlands: ESRO), 39
- Bloomer, J.D., Watson, D.M., Pipher, J.L., Forrest, W.J., Ali, B., Greenhouse, M.A., Satyapal, S., Smith, H.A., Fischer, J., & Woodward, C.E. 1998, *ApJ*, 506, 727
- Carral, P., Kurtz, S.E., Rodriguez, L.F., De Pree, C., & Hofner, P. 1997, *ApJ*, 486, L103
- Carral, P. Kurtz, S.E., Rodriguez, L.F., Menten, K., Canto, J., & Arceo, R. 2002, *AJ*, 123, 2574
- Caswell, J.L. 1997, *MNRAS*, 289, 203
- Cesaroni, R., Churchwell, E., Hofner, P., Walmsley, C.M., & Kurtz, S. 1994, *A&A*, 288, 903
- Claussen, M., Marvel, K.B., Wootten, H.A., & Wilking, B.A. 1997, in IAU Symp.182, Herbig-Haro Flows and the Birth of Low Mass Stars, ed. B. Reipurth & C. Bertout (Dordrecht, The Netherlands: Kluwer), 515
- De Buizer, J.M. 2000, Ph.D. thesis, University of Florida
- De Buizer, J. M., Piña, R.K., & Telesco, C.M. 2000, *ApJS*, 130, 437
- De Buizer, J.M. 2002, in IAU Symp. 206, Cosmic Masers: From Protostars to Blackholes, ed. V. Migenes (San Francisco: ASP), 18
- De Pree, C.G., Rodriguez, L.F., Dickel, H.R., & Goss, W.M. 1995, *ApJ*, 447, 220
- Doyon, R. 1990, Ph.D. thesis, Imperial College, Univ. London
- Ellingsen, S.P., Norris, R.P., & McCulloch, P.M. 1996, *MNRAS*, 279, 101
- Ellingsen, S.P., Norris, R.P., Diamond, P.J., McCulloch, P.M., Amy, S.W., Beasley, A.J., Ferris, R.H., Gough, R.G., King, E.A., Lovell, J.E.J., Reynolds, J.E., Tzioumis, A.K., Troup, E.R., Wark, R.M., & Wieringa, M.H. 1996, in Proceedings of 4th Asia-Pacific Telescope Workshop, ed. E.A. King (ATNF/CSIRO: Sydney), 106
- Emerson, J.P., Jennings, R.E., & Moorwood, A.F.M. 1973, *ApJ*, 184, 401
- Forster, J.R., & Caswell, J.L. 1989, *A&A*, 213, 339
- Gaume, R.A., & Mutel, R.L. 1987, *ApJS*, 65, 193

- Greenhouse, M. A., Woodward, C. E., Thronson, H. A., Rudy, R. J., Rossano, G. S., Erwin, P., & Puetter, R.C. 1991, *ApJ*, 383, 164
- Harvey, P.M., & Gatley, I. 1983, *ApJ*, 269, 613
- Hofner, P., & Churchwell, E. 1996, *A&AS*, 120, 283
- Kraemer, K.E., & Jackson, J.M. 1995, *ApJ*, 439, L9
- Kraemer, K.E., Deutsch, L.K., Jackson, J.M., Hora, J.L., Fazio, G.G., Hoffmann, W.F., & Dayal, A. 1999, *ApJ*, 516, 817
- Kurucz, R.L. 1979, *ApJS*, 40, 1
- Mathis, J.S. 1990, *ARA&A*, 28, 37
- McBreen, B., Fazio, G.G., Stier, M., & Wright, E.L. 1979, *ApJ*, 232, L18
- McKee, C.F., Chernoff, D.F., & Hollenbach, D.J. 1984, in the Sixteenth ESLAB Symposium, Galactic and Extragalactic Infrared Spectroscopy, eds. M.F. Kessler & J.P. Phillips (Dordrecht:Reidel), 103
- Neckel, T. 1978, *A&A*, 69, 51
- Persi, P., Roth, M., Tapia, M., Marenzi, A.R., Felli, M., Testi, L., & Ferrari-Toniolo, M. 1996, *A&A*, 307, 591
- Persi, P., Tapia, M., Felli, M., Lagage, P.O., & Ferrari-Toniolo, M. 1998, *A&A*, 336, 1024
- Rodríguez, L.F., Cantó, J., & Moran, J.M. 1982, *ApJ*, 255, 103
- Tapia, M., Persi, P., & Roth, M. 1996, *A&A*, 316, 102